

## THE QUANTITATIVE ASSESSMENT OF UV EXTINCTION DERIVED FROM *IUE* DATA OF GIANTS AND SUPERGIANTS

JASON A. CARDELLI,<sup>1</sup> KENNETH R. SEMBACH,<sup>1</sup> AND JOHN S. MATHIS

Department of Astronomy, University of Wisconsin-Madison, Madison, Wisconsin 53706

Received 27 April 1992; revised 1 July 1992

### ABSTRACT

In this paper we show that the ultraviolet interstellar extinction towards hot, luminous stars (spectral types B0–B2; MK luminosity classes III–Ia) can be determined as accurately as for hot main-sequence stars. These luminous stars are reasonably numerous and can be observed over large distances and through substantial reddenings. We present an atlas of *International Ultraviolet Explorer* (*IUE*) dereddened fluxes for  $1160 < \lambda < 3125 \text{ \AA}$  of 13 lightly-reddened stars within this temperature/luminosity range, taken from the *IUE* Spectral Atlas of Wu *et al.* [*IUE*, NASA Newsletter, No. 22 (1983)]. These stars form a well-sampled grid (albeit not necessarily uniform) in spectral type and luminosity class and are all suitable comparison stars for the “pair method” of extinction determination. Their fluxes show absorption line strengths that allow a rather accurate *IUE*-based determination of *relative* temperatures and luminosities which is more suitable for the determination of UV extinction via the pair method than choosing a comparison star based only on quoted optical MK classifications. We discuss and tabulate the data used to deredden these standard stars along with dereddening error estimates, as well as the photometric and mismatch errors associated with using these comparison stars to derive extinction curves. We illustrate the accuracy of the method by considering a sample of four reddened luminous stars and conclude that the tabulated and plotted luminous standard star data can be used to produce UV extinction curves as accurate as those found for main-sequence stars.

### 1. INTRODUCTION

Extinction is determined most reliably by the “pair method,” involving a direct comparison of the spectrum of the target or program star to be dereddened and the spectrum of a lightly reddened comparison star (which has itself been dereddened as far as possible) of the same relative spectral type and luminosity class. Employing this technique with early-type main-sequence stars can produce highly reliable results (Massa *et al.* 1983; hereafter MSF; Massa & Fitzpatrick 1986; hereafter MF). However, there are many regions in the Galaxy so distant or heavily reddened that extinction information can only be studied through spectra of high luminosity stars, here defined as MK luminosity classes III–Ia [a major motivation behind the work here arises from a study of extinction in long path length, low density Galactic disk and halo gas which requires the use of luminous stars (Cardelli & Sembach 1992; Cardelli *et al.* 1992)]. Furthermore, sometimes one needs to deredden luminous stars, such as in the Magellanic Clouds, whose individual ultraviolet spectrum can be obtained with instruments like the *International Ultraviolet Explorer* (*IUE*). For such studies it is important to have reliable luminous comparison stars and to also understand the sources and magnitude of the errors associated with extinction derived via supergiants.

The ultimate success in deriving quality UV extinction

results from the pair method requires the proper choice of the comparison star. This requires the establishment of a grid of unreddened or lightly reddened comparison stars that bracket the characteristics of the program star. Historically, early-type main-sequence stars have been the favorite choice because they are relatively numerous, have rather weak absorption lines so that slight spectral type mismatch has little impact on the extinction curve shape (MF; Fitzpatrick & Massa 1990; hereafter FM), and have systematic and well-understood uncertainties associated with temperature mismatch (MSF; MF).

Like the main-sequence stars, giants and supergiants also define a general temperature and luminosity sequence (Fitzpatrick 1988) which is reflected in their UV absorption spectra (Massa 1989; Prinja 1990). However, the spatial density of supergiants is lower than that of main-sequence stars and therefore these stars tend to be distant and reddened by intervening dust. Consequently, there is a general lack of lightly reddened standard stars of many spectral types and high luminosity classes, leading to a general uncertainty in the intrinsic colors of luminous stars. This lack of lightly reddened standards is suggested by the occasional disagreement between the intrinsic colors of various authors (Kester 1981). In addition, abundance peculiarities and possible variability of supergiants in both flux and colors can exist and may be problematic if the effects of such variability are not clearly and uniquely reflected in the absorption spectrum. Finally, unlike the main-sequence stars, the strong luminosity-sensitive UV line blanketing produced by supergiants (Panek & Savage 1976; Koornneef & Code 1981) can produce potentially serious distortions in both the general (e.g., curve shape)

<sup>1</sup>Guest Observers with the *International Ultraviolet Explorer* satellite, which is sponsored and operated by the National Aeronautics and Space Administration, the Science Research Council of the United Kingdom, and the European Space Agency.

and selective (i.e., bump width and position) extinction characteristics for even modest mismatch errors. Because extinction curves derived from low resolution instruments like TD1 and *Astronomy Netherlands Satellite (ANS)* are especially vulnerable to line blanketing effects, extinction derived from supergiants requires extra care.

Supergiants have been used to determine extinction in both the Galaxy (MF) and the LMC (Nandy *et al.* 1981; Koornneef & Code 1981; Fitzpatrick 1985, 1986), and in general the results seem to be consistent and reliable. In addition, Cardelli *et al.* (1989; hereafter CCM) formulated a mean extinction law expressed as a function of the optical parameter  $R(V)$  [ $\equiv A(V)/E(B-V)$ ]. They found no difference in the relationship between  $A(\lambda)/A(V)$  and  $R(V)$  as derived from the sample of Fitzpatrick & Massa (1986, 1988), in which no stars of classes I and only a few of class III were included, and a larger sample of 50 stars observed by *ANS*, containing 10 supergiants. As another example, Savage & Mathis (1979) used compilations containing stars of all luminosities to derive their mean extinction law from data obtained by the TD-1 satellite (Nandy *et al.* 1976) for  $3 \mu\text{m}^{-1} < 1/\lambda < 7 \mu\text{m}^{-1}$ . The Savage—Mathis extinction law illustrates both the good features and the dangers of using luminous stars for determining reddening. On one hand, it provides a good mean of the value expected within the diffuse interstellar medium and agrees very well with the independently derived extinction law of Seaton (1979) and with CCM for a value  $R(V) = 3.2$ . The general agreement of these laws suggests that the inclusion of supergiants does not exert a major disturbing influence on the general shape of the extinction law between the 3000–1200 Å range of (*IUE*). On the other hand, there is a distinct local increase in the Savage—Mathis law around  $1/\lambda = 6.3 \mu\text{m}^{-1}$  ( $\lambda \approx 1600 \text{ Å}$ ) compared to Seaton (1979) or CCM. This spurious feature was produced by mismatch of luminosity sensitive lines (as suspected by Savage and Mathis) and was presumably introduced by Nandy *et al.* (1976) in determining extinctions by comparing stars of differing luminosities.

The above discussion suggests that while extinction derived via supergiants produces generally acceptable results on average, the presence of both temperature and luminosity mismatch clearly makes their use more complicated than for main-sequence stars. The aim of this paper is to quantify just how well luminosity class I–III stars can be used to determine extinction using the *IUE* Standard Star Atlas of Wu *et al.* (1983) as comparison standards. A major goal is to establish a quantitative understanding of the sources and magnitude of the uncertainties for the extinction curve as a whole as has previously been done for extinction derived from main-sequence stars (MSF, MF). We produce a set of dereddened luminous standards which serve to determine accurate extinction properties over the entire wavelength interval 3000–1200 Å for types O9–B2. For completeness, we also include data for class V stars. We also estimate the magnitudes and qualitative effects of errors resulting from random photometric errors, uncertainties in the dereddened colors of standards in the Wu *et al.* atlas, including uncertainties in the adopted intrinsic

TABLE 1. Basic data for *IUE* spectral atlas comparison (standard) stars.

HD	Name	Spectral Type	Ref. <sup>a</sup>	V	U-B	B-V	Ref. <sup>b</sup>	S <sup>c</sup>	L <sup>d</sup>
47839	15 Mon	O7 V((f))	W72	4.65	-1.06	-0.25	J55	0.943	1.064
214680	10 Lac	O9 V	W71	4.88	-1.04	-0.20	Nic	0.933	1.077
38666	$\mu$ Col	O9.5 IV	W73	5.17	-1.06	-0.28	Nic	0.936	1.074
188209		O9.5 Ia	L	5.62	-0.97	-0.07	Nic	0.951	1.054
36512	$\nu$ Ori	B0 V	W71	4.62	-1.07	-0.26	Nic	0.986	1.015
63922		B0 III	HGS	4.11	-1.01	-0.18	Nic	0.987	1.013
204172	69 Cyg	B0 Ib	L	5.94	-0.94	-0.08	Nic	0.986	1.015
55857		B0.5 V	HGS	6.11	-0.99	-0.26	CS	0.977	1.024
119159	64760	B0.5 III	HGS	6.00	...	-0.08	Nic	1.005	0.995
150898		B0.5 Ib	HGS	4.24	-1.00	-0.14	Nic	0.981	1.020
		B0.5 Ia	HGS	5.58	-1.00	-0.08	Nic	0.971	1.031
31726	$\epsilon^1$ CMa	B1 V	L	6.15	...	-0.21	Nic	0.963	1.040
46328		B1 III	HGS	4.33	-0.98	-0.24	J66	0.986	1.015
40111	139 Tau	B1 Ib	L	4.82	-0.93	-0.06	Nic	0.952	1.054
91316		B1 Iab	L	3.85	-0.96	-0.14	Nic	0.951	1.055
150168	$\rho$ Leo	B1 Ia	HGS	5.65	-0.87	-0.03	Nic	1.005	0.996
74273	62747	B1.5 V	HGS	5.90	-0.90	-0.21	Nic	0.967	1.035
62747		B1.5 III	HGS	5.62	...	-0.19	Nic	0.978	1.023
64802	$\zeta$ Cas	B2 V	HGS	5.49	-0.73	-0.19	Nic	0.969	1.033
3360		B2 IV	L	3.66	-0.87	-0.20	Nic	0.981	1.020
51283	165024	B2 III	HGS	5.28	...	-0.19	CS	0.972	1.030
165024		B2 Ib	HGS	3.66	-0.85	-0.08	Nic	0.991	1.010

#### Notes to TABLE 1

<sup>a</sup>Spectral type references: HGS, Hitner *et al.* (1969); L; Lesh (1968); W71, Walborn (1971); W72, Walborn (1972); W73, Walborn (1973).

<sup>b</sup>Photometry references: CS, Cousins & Stoy (1962); J55, Johnson (1955); J66, Johnson (1966); Nic, Nicolet (1978).

<sup>c</sup>Ratio of the average flux in the overlap region between the two camera images to the SWP flux corresponding to wavelengths where the data quality are considered good (see Bohlin *et al.* 1990). The SWP data were subsequently scaled by this factor prior to being merged with the LWR data (see Sec. 2).

<sup>d</sup>Ratio of the average flux in the overlap region between the two camera images to the LWR flux corresponding to wavelengths where the data quality are considered good (see Bohlin *et al.* 1990). The LWR data were subsequently scaled by this factor prior to being merged with the SWP data (see Sec. 2).

colors, and spectral type and luminosity class mismatch between program and comparison stars.

## 2. *IUE* SPECTRAL ATLAS DATA

Extinction studies using giants and supergiants require a two-dimensional grid of good quality, comparison star spectra representing a range of both temperature and luminosities. We have chosen the data available in the *IUE* Standard Star Atlas (Wu *et al.* 1983), a sample of stars that are both well-observed and reasonable representatives of individual spectral types and luminosity classes. (We note that these atlas stars are not MK standards and so do not necessarily represent an evenly sampled grid of temperatures and luminosities.) Basic data for our stars are given in Table 1. Although the specific focus here is stars of class I–III, we include representative examples of class V as well for completeness. The data listed in Table 1 include spectral types,  $V$  magnitudes, observed  $U-B$  and  $B-V$  colors, and references. The quoted spectral types were obtained from Lesh (1968), Hitner *et al.* (1969), and Walborn (1971, 1972, 1973).

The low-dispersion data utilized in this study were obtained from the *IUE* archives and were processed with Version 2 of the standard spectral extraction and processing routines available at the Goddard Space Flight Center.

The philosophy behind the data reduction process is given in Turnrose & Thompson (1984). Boggess *et al.* (1978a, 1978b) give details about the *IUE* spacecraft and its detectors. Information regarding the acquisition, type, exposure times, and quality of the individual exposures can be found in the Wu *et al.* (1983) atlas for which the data were originally obtained. All subsequent display and processing of the data was performed with software available on a VAX 4000 at the Midwest Astronomical Data Reduction and Analysis Facility in Madison, Wisconsin.

The individual extracted Short Wavelength Prime (SWP) and Long Wavelength Redundant (LWR) spectra were corrected for camera head amplifier sensitivity following the standard RDAF procedures. Short duration exposures were obtained in a trailed mode within the large aperture. Exposure times less than 60 seconds were corrected for exposure time quantization. The corrected exposure times and the absolute flux calibration of Bohlin & Holm (1980) appropriate for trailed images were used to determine the absolute flux levels for data obtained with both cameras.

The SWP and LWR data were also corrected for long-term camera sensitivity degradation according to the procedures described in Bohlin & Grillmair (1988a, 1988b; see also Clavel *et al.* 1988; Holm 1985; Sonneborn & Garhart 1987). Since all of the exposures for stars in the Wu *et al.* atlas were obtained prior to 1983, the long term camera sensitivity degradation corrections were typically only a few percent at most wavelengths.

Blemishes resulting from detector reseaux marks were removed from the data by linearly interpolating across the features. The 2200 Å “hot spot” present in the LWR spectra was also removed by linear interpolation between the nearest unaffected pixels. The extent of the feature was typically 8 to 10 Å wide.

The individual extracted SWP and LWR spectra were binned at 3 Å intervals. This binning size preserved the spectral resolution ( $R \sim 300\text{--}1000$ ) of the unbinned data. An inspection of the individual SWP and LWR spectra indicated a vertical offset between the two cameras of the order of 6%–8% which is evident in the Wu *et al.* (1983) atlas figures. We chose to remove this shift by scaling the LWR and SWP data to the relative mean in the 1900–2000 Å overlap region. The shifts required in each case are listed in the last two columns of Table 1. The source of these shifts may be related to the fact that all the data in our sample were trailed spectra (see Bohlin *et al.* 1990). Further discussion of these shifts will be given in a forthcoming paper.

The data for the four program stars discussed in Sec. 4 required a slightly more sophisticated reduction process. However, the general outline discussed above, including the image shifts, was employed. Specific details regarding the processing for those stars can be found in Cardelli & Sembach (1992).

### 3. COMPARISON (STANDARD) STAR CHARACTERISTICS

In the derivation of extinction curves via the pair method, the appropriate comparison star is best deter-

mined by matching its observed stellar absorption features to those for the program star since it is assumed that two stars exhibiting (nearly) identical absorption spectra will have (nearly) identical temperatures and luminosities and hence (nearly) identical intrinsic flux distributions. In this section, we present an atlas of giant and supergiant comparison stars and discuss specific characteristics associated with their use as extinction standards. In all following discussions, we shall continue to reference individual stars by their spectral and luminosity classes as given in Table 1, despite the fact that the assignment of these spectral types may not be completely consistent with the observed UV spectrum or the true absolute MK classification. Since we are specifically interested in the use of these stars as UV extinction standards, we are only concerned with matching spectral characteristics between the program and comparison stars. In other words, *we are not concerned with whether or not the quoted optical or inferred UV classification for a specific standard exactly conforms to an absolute MK classification, but rather that its UV absorption spectrum conforms to a flux distribution shared by stars with similar absorption spectra.*

#### 3.1 Dereddening

In this section, we consider the reddening of the comparison stars and attempt to understand the impact that reddening has on their intrinsic flux distributions. Throughout the discussions below, we refer to the wavelength dependent extinction in the form  $E(\lambda) \equiv E(\lambda - V) / E(B - V)$ . Also, terms associated with the comparison star dereddening carry the subscript “c.”

The first step in assessing comparison star UV reddening is to determine the amount of visual reddening,  $E(B - V)_c$ , by comparing the observed  $B - V$  with  $(B - V)_0$ , the intrinsic color appropriate to the quoted spectral type and luminosity class. For the data in Table 1, we adopt the  $(B - V)_0$  colors of Johnson (1958) and FitzGerald (1970). [Note that this is the only instance where we actually rely directly on the absolute spectral types for the comparison stars. The consequences of this reliance on  $(B - V)_0$  is discussed in Sec. 3.2.]

The next step is to determine the reddening of the standard stars,  $E(\lambda)_c$ . The traditional approach has generally been to assume some  $E(\lambda)$  such as that of Savage & Mathis (1979) or Seaton (1979) and incorporate potential uncertainties due to this assumption into the error analysis of the program star extinction curve derived from using the comparison star (see MF). For the stars with  $E(B - V)_c < 0.05$ , we adopt the  $R(V)$ -dependent average from CCM appropriate to  $R(V) \approx 3.1$ , which is similar to the average curve of Savage & Mathis (1979) and Seaton (1979). However, for  $E(B - V)_c > 0.05$ , we have estimated the extinction for each standard star, especially the strength of the  $\lambda 2175$  bump, which exhibits variations even among sightlines with the same  $R(V)$  (Mathis & Cardelli 1992; see also the standard deviations shown in Fig. 4 of CCM).

The first method of dereddening standard stars requires that the dereddened *IUE* flux of a particular reddened

standard star represent a fairly smooth interpolation between the dereddened fluxes of the less reddened standards that bracket the particular star in both spectral type and luminosity class. We start with the standards with  $E(B-V)_c$  slightly larger than 0.05. Since the standard stars with  $E(B-V)_c \leq 0.05$  cover only a coarse grid of spectral types and luminosity classes, their use constitutes appreciable mismatch errors. However, if the comparison star is hotter than the reddened standard star, the derived  $E(\lambda)$  will uniformly rise too steeply with increasing wave number, and conversely if the comparison star is too cool (see, for example, Figs. 1 and 2 in Cardelli & Clayton 1991). The relative temperatures of the reddened and unreddened standards are known from the spectral types and luminosity classes and are exhibited by the UV absorption spectrum. The estimate of  $E(\lambda)_c$  for each reddened standard star is chosen by requiring that the star's dereddened flux distribution be bracketed from above by the hotter dereddened standards and from below by the cooler with the dereddened flux obtained by an interpolation between them. *The relative spectral types are judged by the UV line strengths, not the assigned MK class, whenever the two are in conflict.* (See Sec. 3.2 below.) This procedure effectively requires the dereddened fluxes to show a regular progression as either the spectral type is varied at a constant luminosity class or the luminosity class is varied at a given spectral type. The strength of the bump is adjusted individually for each reddened standard star in order to make the dereddened flux near 2175 Å have the same shape as the fluxes of slightly warmer or cooler stars. We apply this method to each of the standard stars in increasing order of their reddening. After the  $E(\lambda)_c$  for a standard star is adopted, that star's dereddened flux is used for comparison with more heavily reddened standards. We note that this approach may introduce systematic uncertainties since our standard star data are not actually MK standards and hence do not necessarily represent an evenly spaced grid in either temperature or luminosity. However, the impact that these uncertainties will have on derived program star extinction are consistent with general continuum mismatch errors (see Secs. 4.3 and 4.4 below). These uncertainties are included with the general comparison star dereddening errors which are discussed in Sec. 3.3 below.

The second general method of dereddening standard stars is to use the *ANS* catalog of Savage *et al.* (1985), who assessed the extinction of 1415 stars, predominantly representing lines of sight through the diffuse interstellar medium (ISM) [ $R(V) \approx 3.1-3.2$ ]. Extinction for the individual entries in the catalog, which were subjected to strict choice criteria, was derived through a comparison with the intrinsic colors of Wu *et al.* (1980), obtained by use of the well-determined mean *ANS* extinction law appropriate to the diffuse ISM. The *ANS* filter observations, at 3294, 2493, 2200, 1799, and 1549 Å, provide accurate estimates of the bump strengths for our reddened standard stars. Following Fitzpatrick & Massa (1986), we estimate the  $E(\lambda)_c$  of the reddened standard by fitting the *ANS* results with an extinction linear in  $1/\lambda$  between 3294 and 1549 Å, plus a bump to fit the 2200 Å extinction.

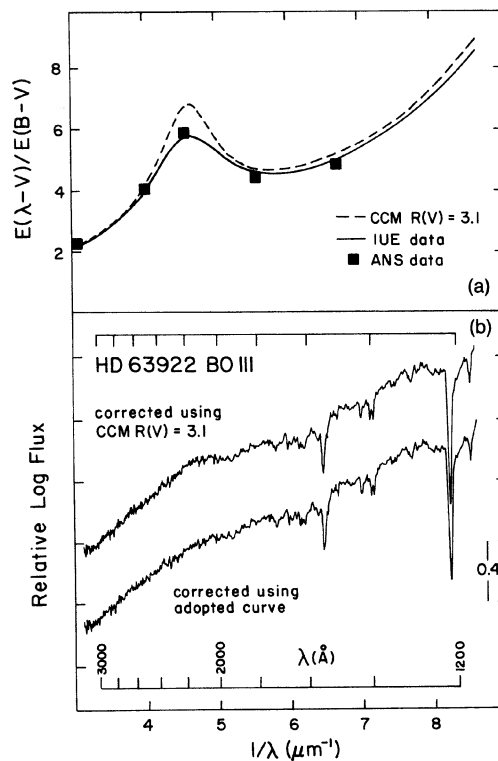


FIG. 1. (a) Comparison between the general shape of the extinction curve for the B0 III standard star HD 63922 [ $E(B-V)_c=0.12$ ] derived from a comparison to more lightly reddened standards in our sample [e.g., HD 38666, O9.5 IV,  $E(B-V)_c=0.02$ ; HD 55857, B0.5 V,  $E(B-V)_c=0.02$ ] plotted as a solid line, the *ANS* extinction data for HD 63922 taken from Savage *et al.* (1985) plotted as filled symbols, and the  $R(V)=3.1$  extinction curve from Cardelli *et al.* (1989) plotted as a dashed line. (b) The logarithm of the relative flux distribution for HD 63922 corrected for reddening using the  $R(V)=3.1$  extinction curve (top plot) compared to the one corrected using the adopted extinction curve from Table 2 (bottom plot) plotted against  $1/\lambda$  ( $\mu\text{m}^{-1}$ ). The data corrected with the  $R(V)=3.1$  curve appears significantly over-corrected in the bump region.

An example of the results of using both the *IUE* and *ANS* data sets to assess the extinction is shown in Fig. 1(a) for HD 63922 (B0 III). The solid line represents the mean extinction adopted from our bracketed mismatch using the *IUE* data while the filled symbols correspond to the *ANS* extinction from Savage *et al.* (1985), shifted vertically by +0.3 mag. [Because the reddenings are small, such a shift is consistent with general photometric uncertainties as discussed in Sec. 4.1.] The dashed curve represents the CCM  $R(V)$ -dependent curve for  $R(V)=3.1$ . The agreement between the *IUE* and *ANS* extinction in this case is quite good. However, note that the derived extinction deviates significantly from the  $R(V)=3.1$  curve in the region of the bump. The impact of the individual  $E(\lambda)_c$  on the reddening corrected flux is shown in Fig. 1(b), where the reddening-corrected fluxes are plotted against  $x \equiv 1/\lambda$  ( $\mu\text{m}^{-1}$ ). The top spectrum was derived by using the CCM  $R(V)=3.1$  curve while the bottom was derived by using

TABLE 2. Adopted comparison (standard) star reddening data.

HD	Type <sup>a</sup>	Source <sup>b</sup>	Adopted UV Reddening Curve Data <sup>c</sup>				
			$\gamma$	$c_1$	$c_2$	$c_3$	$c_4$
47839	O7 V((f))	ANS	1.00	-0.30	0.80	2.90	0.75
214680	O9 V	ANS/IUE	1.00	-0.80	0.95	2.72	0.53
38666	O9.5 IV	e	1.00	-0.24	0.74	3.56	0.52
188209	O9.5 Ia	ANS/IUE	1.00	-0.65	0.90	3.20	0.49
36512	B0 V	e	1.00	-0.24	0.74	3.56	0.52
63922 <sup>d</sup>	B0 III	ANS/IUE	1.20	-0.17	0.69	3.80	0.48
204172	B0 Ib	ANS/IUE	0.80	-1.70	1.25	2.00	0.60
55857	B0.5 V	e	1.00	-0.24	0.74	3.56	0.52
119159	B0.5 III	ANS/IUE	1.00	-0.44	0.81	3.70	0.45
64760 <sup>d</sup>	B0.5 Ib	ANS	1.30	-0.31	0.77	3.65	0.53
150898	B0.5 Ia	ANS/IUE	0.92	-0.27	0.74	4.00	0.54
31726	B1 V	ANS	1.00	-0.17	0.71	2.82	0.51
46328	B1 III	e	1.00	-0.24	0.74	3.56	0.52
40111	B1 Ib	ANS/IUE	1.00	-0.03	0.65	4.49	0.49
91316	B1 Iab	ANS	1.40	-3.30	1.81	4.10	0.50
150168	B1 Ia	ANS/IUE	1.00	-0.12	0.68	5.00	0.57
74273	B1.5 V	e	1.00	-0.24	0.74	3.56	0.52
62747	B1.5 III	ANS	1.00	0.52	0.48	2.80	0.40
64802 <sup>d</sup>	B2 V	ANS	1.20	-0.11	0.69	3.80	0.47
3360	B2 IV	e	1.00	-0.24	0.74	3.56	0.52
51283	B2 III	ANS	1.00	-0.24	0.74	3.40	0.52
165024	B2 Ib	ANS/IUE	1.00	0.81	0.42	4.50	0.35

## Notes to TABLE 2

<sup>a</sup>Quoted spectral types from Table 1. The appropriate color excesses can be found from the data in Table 1 and Table 3 (see Sec. 3.2).

<sup>b</sup>Source of UV extinction curve information. The *ANS* notation corresponds to data taken from the *ANS* extinction excess catalog of Savage *et al.* (1985). The *IUE* notation refers to information assessed from comparison to *IUE* spectra (see text).

<sup>c</sup>Adopted parametrized extinction data following the formulation of Fitzpatrick & Massa (1988, 1990). For all cases, the bump centroid term corresponds to  $\lambda_0^{-1} = 4.59 \mu\text{m}^{-1}$ . The basis for these adopted curves derives from a comparison of the (modified)  $R(V)$ -dependent extinction law of Cardelli *et al.* (1989) in the form  $E(\lambda - V)/E(B - V)$  and the extinction assessed from the sources listed in column 4 (see text).

<sup>d</sup>These three stars correspond to sight lines in the Gum nebula and their inferred bump characteristics are similar to those exhibited by Gum nebula sight line toward HD 62542 (Cardelli & Savage 1988).

<sup>e</sup>Curve assumed to take the form of the  $R(V)$ -dependent extinction law of Cardelli *et al.* (1989) for  $R = 3.1$ .

the reddening inferred from the *IUE* and *ANS* analysis. The top spectrum appears significantly over-corrected in the 2200 Å region and is a prime example of why we chose to derive first order extinction estimates instead of simply adopting an average curve.

To describe the adopted  $E(\lambda)_c$ , we utilize the parametrization of FM:  $E(\lambda) = c_1 + c_2x + c_3B(x, \lambda_0^{-1}, \gamma) + c_4F(x)$ , where  $B(x, \lambda_0^{-1}, \gamma)$  is the bump profile,  $F(x)$  is the far-UV curvature function,  $\lambda_0^{-1}$  is the bump centroid, and  $\gamma$  is the bump width parameter. In most instances where results from both *IUE* and *ANS* data could be derived, the relative agreement was quite good [i.e., Fig. 1(a)]. In cases where the *IUE* and *ANS* results differed, we adopted a simple mean for  $c_1$ ,  $c_2$ , and  $c_3$ . With six exceptions (see Table 2), our analysis was insensitive to  $\gamma$  and  $\lambda_0^{-1}$ , and we adopted  $\gamma = 1.0$  and  $\lambda_0^{-1} = 4.59 \mu\text{m}^{-1}$  which are typical values for diffuse cloud extinction. Uncertainties in these two parameters appear to have little effect on corrected comparison star fluxes or the general shape of the extinction curve derived from using the reddening-corrected comparison star. However, uncertainties in these values can have an

effect on the determination of  $\gamma$  and  $\lambda_0^{-1}$  for an arbitrary program star. The nature and impact of these uncertainties are discussed in more detail in Cardelli & Sembach (1992).

We fitted the final  $E(\lambda)_c$  with the CCM  $R(V)$ -dependent extinction law in the form of the FM parametrization, with modifications applied to the CCM bump and far-UV terms where necessary. For the majority of cases, the implied  $R(V)$  value was of the order of 2.8–3.4. The resulting adopted first-order reddening data for the comparison stars listed in Table 1 are given in Table 2.

Our principal purpose in deriving first-order estimates of the comparison star reddening was to produce a set of intrinsic fluxes that are more accurate (with respect to dereddening) than would be found if we simply adopted a standard diffuse interstellar extinction law. However, a plot of the data in Table 2 shows that the adopted results are generally consistent with these “standard” laws except for the bump, which shows variations of about  $\pm 20\%$  about the average. This variation is typical for extinction curves corresponding to the implied range of  $R(V)$ , 2.8–3.4 (see CCM), characteristic of extinction in the moderately low density diffuse ISM. For our comparison star data, we find  $E(B - V)/r \approx 0.10 \pm 0.05$  mag/kpc which is consistent with sampling fairly low mean sight line densities. Consider for comparison the general extinction sample of Fitzpatrick & Massa (1986) which cover a similar range in distance and for which all but three of 45 sight lines have  $E(B - V)/r > 0.15$  mag/kpc.

Two other stars in Table 2, HD 64760 (B0.5 Ib) and HD 64802 (B2 V), have extinction with weak, broad bumps similar to that of HD 63922 shown in Fig. 1(a). The sight lines to all three stars pass into or through the Gum nebula complex and share similar bump extinction characteristics to HD 62542, another Gum nebula sight line with well-determined extinction characteristics (Cardelli & Savage 1988). The general similarity between these four sight lines and their association with a single complex supports the validity of our adopted extinction curves for these three stars. Furthermore, the results for these four sight lines seem to suggest that weak bump extinction is endemic to the Gum nebula complex in general.

### 3.2 Intrinsic Stellar Characteristics: Absorption Lines and Flux Distributions

The reddening corrected comparison star spectra are shown in Figs. 2–4 for luminosity classes V, III, Ib, and Ia/ab, respectively. The spectra show a distribution of absorption features with a wide range of sensitivities to variations in both temperature and luminosity. [General discussions about the UV absorption line identification and temperature/luminosity sensitivities can be found in Panek & Savage (1976), Koornneef & Code (1981), Heck (1987), Massa (1989), and Prinja (1990).] In Figure 5 we show the spectrum of HD 91316 (B1 Iab) along with identifications of the major spectral features. The notion “Fe III” indicates the blend of a number of individual features. The positions marked with an “e” correspond to the position of emission from P-Cygni profiles for C IV, Si IV, and

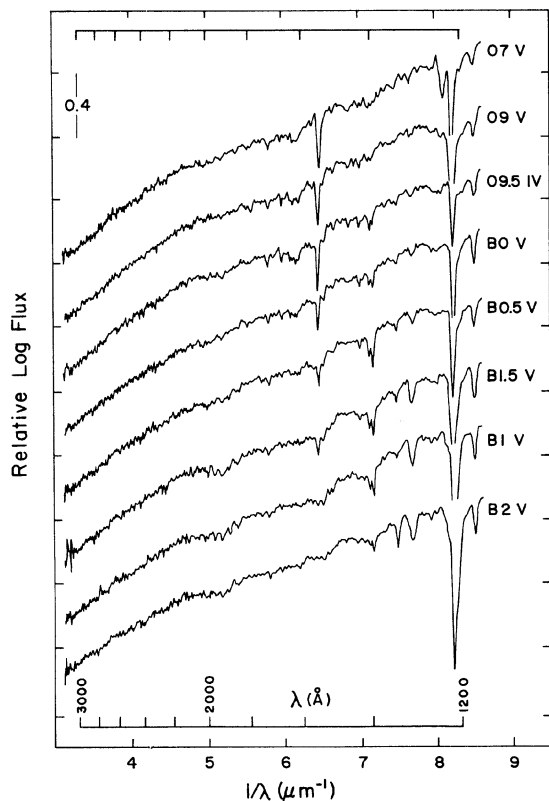


FIG. 2. The logarithm of the relative flux distributions for the class V comparison stars, corrected for reddening using the adopted extinction data in Table 2, plotted against  $1/\lambda$  ( $\mu\text{m}^{-1}$ ). The spectra have been ranked in the plot according to the *relative* spectral type suggested by the UV absorption spectra which is not necessarily consistent with the quoted optical spectral types given in Tables 1 and 2.

N v as can be seen in Fig. 4(b) for the O9.5 Ia spectrum. The principal intent of this section is to establish some basic criteria that will be useful for the unambiguous identification of giants and supergiants.

In general, the characteristics of the class V stars are fairly well determined and Fig. 2 provides a useful guide to understanding how specific spectral features such as C IV, Si IV, C II, and Si II/III depend upon variation in temperature only. How these and the other features identified in Fig. 5 depend upon both temperature and luminosity is shown in Fig. 6 where we plot the range of luminosity classes for types B0 and B2. These spectral types bracket the temperature range of our class III and I stars. While most of the absorption features exhibit a dependency on both temperature and luminosity, considering various features together can provide useful information when assigning a spectral classification. For example, comparing Fig. 6 with Fig. 2 shows that even though C IV, Si IV, and N v are strongly dependent on both temperature and luminosity, these features have limited use in discriminating luminosity class III and I objects from class V. For the class V stars represented here, these features show a strong dependence on temperature, with C IV and N v being strongest in the

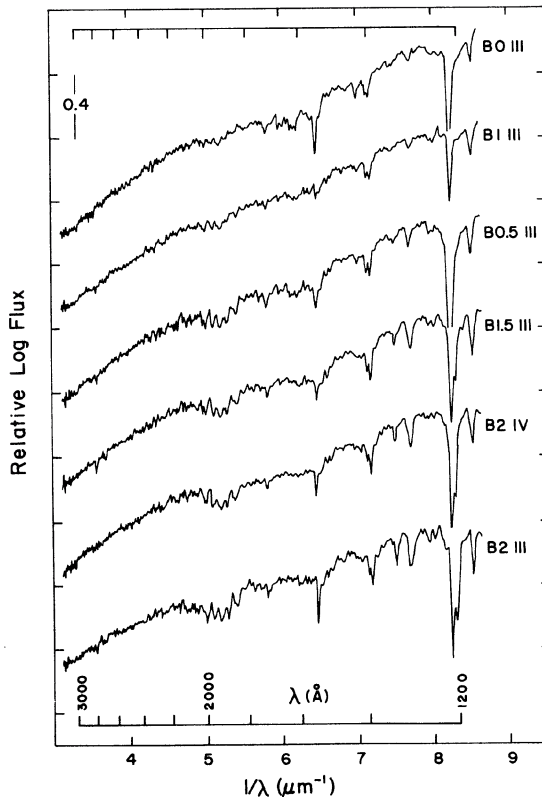
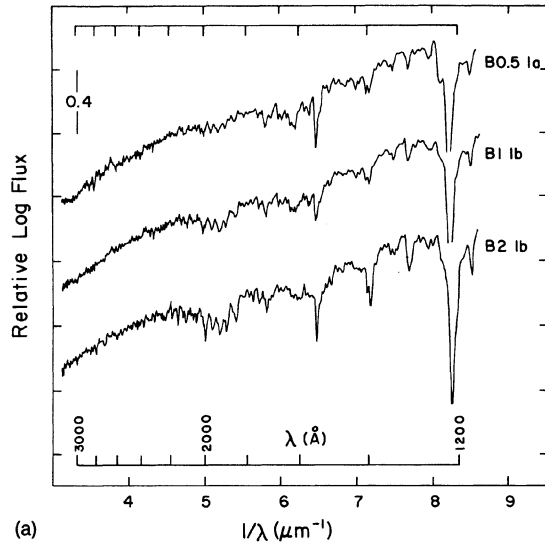


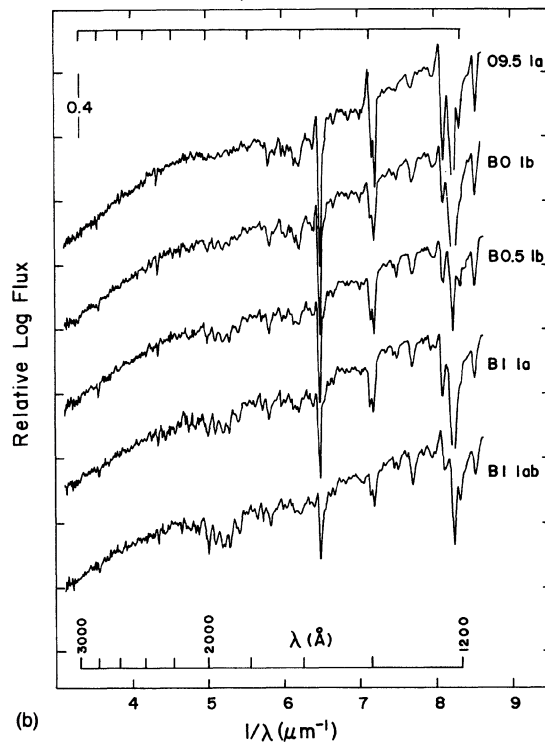
FIG. 3. Same as Fig. 2 except for the class III comparison stars. The inclusion of the B2 IV (HD 3360) star in this plot derives from the fact that its UV absorption spectrum appears more consistent with the other class III stars than with the class V stars.

late O stars while Si IV reaches peak strength in the early B stars. Among types III and I, these features are not very good discriminators of temperature as can be seen by comparing the B0 III and B2 III stars in Fig. 6. However, if the C II and Si II/III features, which are primarily temperature sensitive, are included in the classification scheme, the differences between the B0 III and B2 III comparison star spectra are readily apparent.

As another example, consider the “Fe III”, adjacent Al III, N IV/C II/Al II, and Fe III/Al III features. For class V stars, these features are weak or absent for all spectral types of interest here. However, for classes III and I, these features can become quite strong. The N IV/C II/Al II blend shows a modest positive luminosity effect but is nearly constant in strength for different spectral types (temperature) within the same luminosity class. The “Fe III” blend and adjacent Al III feature show a strong positive luminosity effect between class V and III–I and a much weaker dependence between class III and I. However, these features show a strong dependence on *decreasing* temperature, becoming quite prominent for spectral types later than B1. On the other hand, the Fe III/Al III blend, which exhibits a modest positive luminosity effect between all luminosity classes, shows a fairly strong dependence on *increasing* temperature becoming strongest in spectral types earlier than B1 for all luminosity classes.



(a)



(b)

FIG. 4. Same as Fig. 2 except for the class I stars. Based on the strength of luminosity-sensitive absorption features, particularly C IV, Si IV, and N V, the class I data are plotted as (a) class Ib and (b) class Iab-a. As in Figs. 2 and 3, the ranking implied by the UV absorption lines is inconsistent with the ranking implied by quoted optical spectral type for several cases.

When considered by themselves, the individual features and blends provide limited discrimination of variations in both temperature and luminosity (e.g., the strong presence of the “Fe III” blend indicates luminosity classes III–I and spectral types later than B1 while the strong presence of Al II and Fe III/Al III indicates classes Ib–Ia and spectral types earlier than B1). However, when considered to-

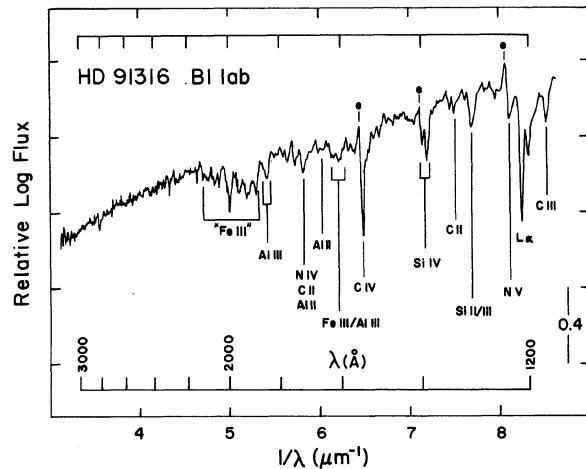


FIG. 5. The logarithm of the relative flux of the B1 Iab comparison star HD 91316, corrected for reddening using the adopted extinction data in Table 2, plotted against  $1/\lambda$  ( $\mu\text{m}^{-1}$ ). Individual absorption features or blends are labeled. The dependencies of these features on temperature and luminosity are discussed in Sec. 3.2. The positions marked “e” correspond to emission from P-Cygni profiles.

gether, the array of features identified in Fig. 5 provide sufficient information from which to accurately assess both *relative* temperature and luminosity class.

For the data plotted in Figs. 2–4, we used the absorption line criteria discussed above to produce a *relative* ranking of the spectra within each luminosity group in decreasing temperature from top to bottom. In addition, we also used available  $c_1$  and  $\beta$  photometric data (Lindemann & Hauck 1973) and the analyses of Massa (1989) and Prinja (1990), based on high dispersion *IUE* data, to assess the *relative* temperature and luminosity designations. While this ranking is generally reflected in the run of quoted optical MK spectral types, there are examples where the temperature ranking inferred from the quoted spectral type is inconsistent with the ranking found from the UV absorption spectra. Similar inconsistencies are also indicated for the luminosity class designations. For example, among our class V stars, the absorption spectra of our B1 and B1.5 stars (HD 31726 and HD 74273, respectively) clearly indicate a relative temperature ranking that is inverted from that implied by the spectral types. Among our class III stars, the Si II/III absorption in the B1 III spectrum (HD 46328) indicates a higher temperature than the B0.5 III (HD 119159) while the strength of the Fe III/Al III feature appears to be somewhat weaker than is seen for our other class III stars. Cross-reference to our sample of class V stars suggests that its UV absorption is more similar to B0.5–1 in this group. Conversely, comparison of our B0.5 III spectrum to the other classes suggests that it may be somewhat cooler (B0.5–1?) and more luminous (III–II?). Finally, the general strength of luminosity-sensitive features, especially C IV, Si v, and N v, in the supergiant spectra provide a relative discrimination between Ib and Iab/a. Consequently, in Figs. 4(a) and 4(b) the quoted luminosity classifications are mixed in both figures.

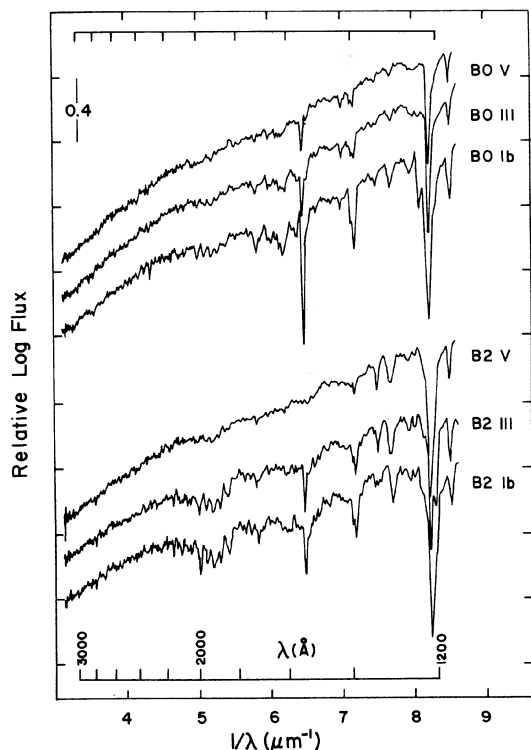


FIG. 6. The logarithm of the relative flux for range of luminosity classes for B0 and B2, corrected for reddening using the adopted extinction data in Table 2, plotted against  $1/\lambda$  ( $\mu\text{m}^{-1}$ ). The purpose of this plot is to show how the various UV absorption features depend on both temperature and luminosity (see Fig. 5 for the identifications of the various features).

Because our use of the pair method is based strictly on finding the best spectral match between program and comparison star, inconsistencies or inaccuracies in assigned classifications are unimportant with respect to the UV data. However, since we must utilize an intrinsic color,  $(B-V)_0$  to derive  $E(B-V)$ , we must rely on some assigned classification as stated in Sec. 3.1. We must therefore consider the impact of possible uncertainties in the assigned classifications. From a comparison of the absorption line information for the data in Figs. 2–4 in conjunction with the analyses of Massa (1989) and Prinja (1990), we estimate possible “alternate” classifications and list the results in Table 3. These “alternate” classifications are not intended to represent true classifications, but rather to simply explore possible uncertainties in  $(B-V)_0$ . The classifications from Table 1 along with the corresponding values of  $(B-V)_0$  from Johnson (1958) and FitzGerald (1970) are given in columns 2 and 3, respectively. The “alternate” classifications estimated from the data along with the values of  $(B-V)_0$  corresponding to the mean of the range are given in columns 4 and 5. The corresponding color difference is listed in column 6. For the most part, the variances from the quoted classifications are small in both spectral type and luminosity class. The variation of  $(B-V)_0$  is also generally small and so use of the quoted spectral types to obtain an intrinsic  $(B-V)_0$  should not produce significant

TABLE 3. Intrinsic color uncertainties associated with variances in assigned spectral types.<sup>a</sup>

HD	Spectral Type <sup>b</sup>	$(B-V)_0^c$	Alternate <sup>d</sup>	$(B-V)_0^e$	$\Delta(B-V)_0^f$
47839	O7 V	-0.32	...	...	...
214680	O9 V	-0.31	...	...	...
38666	O9.5 IV	-0.30	...	...	...
36512	B0 V	-0.30	...	...	...
55857	B0.5 V	-0.28	...	...	...
31726	B1 V	-0.26	...	...	...
74273	B1.5 V	-0.25	B1.5-1 IV-III	-0.26	0.01
3360	B2 IV	-0.24	B2-1.5 III	-0.25	0.01
64802	B2 V	-0.24	...	...	...
63922	B0 III	-0.30	B0-0.5 III-IV	-0.29	-0.01
119159	B0.5 III	-0.28	B0.5-1 III-II	-0.26	-0.02
46328	B1 III	-0.26	B1-0.5 IV	-0.27	0.01
62747	B1.5 III	-0.25	...	...	...
51283	B2 III	-0.24	B2-2.5 III-II	-0.21	-0.03
204172	B0 Ib	-0.23	B0-0.5 Ia	-0.22	-0.01
64760	B0.5 Ib	-0.21	B0.5-1 Iab	-0.20	-0.01
40111	B1 Ib	-0.19	B1-0.5 Ib	-0.20	0.01
165024	B2 Ib	-0.17	B2-2.5 Ib-Iab	-0.16	-0.01
188209	O9.5 Ia	-0.26	O9.5 Iab	-0.26	0
150898	B0.5 Ia	-0.21	B0.5-0 Ib-Iab	-0.22	0.01
150168	B1 Ia	-0.19	...	...	...
91316	B1 Iab	-0.19	B1-2 Iab-Ia	-0.18	-0.01

Notes to TABLE 3

<sup>a</sup>The “alternate” classifications are not presented as true absolute adjustments to the classifications but rather as a means to explore possible variances in the adopted  $(B-V)_0$  colors.

<sup>b</sup>Spectral type/luminosity class taken from sources in Table 1.

<sup>c</sup>Intrinsic colors from Johnson (1958) and FitzGerald (1970).

<sup>d</sup>Possible alternate spectral type/luminosity classes or ranges assessed from the intercomparison of the UV absorption spectra of all the reddening corrected data within and across the luminosity sequences, from [c1] and  $\beta$  photometry, and from the analyses of Massa (1989) and Prinja (1990). These alternative types are intended only as a way to explore potential uncertainties in the adopted  $(B-V)_0$  colors.

<sup>e</sup>Intrinsic  $(B-V)_0$  values correspond to the mean for the quoted alternate type/range.

<sup>f</sup>Difference in the intrinsic  $(B-V)_0$  between the adopted and alternate spectral types/range. The purpose is to assess the size of the uncertainty in  $(B-V)_0$  associated with an incorrect assignment relative to the general spectral type/luminosity sequence.

errors (the impact of these color uncertainties is discussed below).

### 3.3 Comparison Star Dereddening Errors

Our primary goal in determining first-order reddening corrections is to produce a best estimate of the *general shape of the true reddening curve*. While we cannot confirm the absolute accuracy of the adopted reddening corrections, intercomparison of the reddening corrected spectra suggest that no significant localized extinction deviations such as those seen in Fig. 1(b) are present. Thus, we believe that *our adopted extinction better represents the shape of the true wavelength dependence on average than would be expected had we simply adopted an average curve*. However, we recognize that general systematic errors in the adopted  $E(\lambda)_c$  may exist and that it is important to consider the form of this uncertainty,  $\pm \Delta E(\lambda)_c$ , since it will have an impact on the extinction curves derived from the use of the comparison stars.

From our analysis of the comparison star reddening, we find that the uncertainty in the adopted  $E(\lambda)_c$  takes the form of a general increasing or decreasing slope with increasing  $1/\lambda$  which to first order can be represented by a

simple scaling of  $E(\lambda)_c$ . It can be shown that such behavior can arise from both mismatch and uncertainty in  $E(B-V)_c$  (see for example Figs. 1 and 2 in Cardelli & Clayton 1991). To quantitatively represent the effects of this “scaling” uncertainty on  $E(\lambda)_c$ , we employ the  $R(V)$ -dependent extinction law of CCM which takes the form  $A(\lambda)/A(V) = a(x) + b(x)/R(V)$ , where  $x \equiv 1/\lambda$ . With respect to the extinction normalization we employ here, this extinction law takes the alternate form  $E(\lambda) \equiv [E(\lambda - V)/E(B - V)] = [a(x) - 1]R(V) + b(x)$ . Since the nature of the  $R(V)$ -dependence itself mimics the wavelength dependent form of the errors discussed above (e.g., see Fig. 4 in CCM), we can approximate  $\Delta E(\lambda)_c$  by adopting a variance in  $R(V)$ , or  $\Delta E(\lambda)_c \approx \Delta R(V)[a(x) - 1]$ . From an examination of the variances seen in our analysis of the extinction determined from both the *IUE* and *ANS* data, we conservatively adopt  $\Delta R(V) \approx \pm 0.3$ .

Expressing  $\Delta E(\lambda)_c$  in this form is useful since this expression does not require an actual knowledge of  $R(V)$  and the “errors” are applied equally, independent of  $R(V)$ . In addition, since  $\Delta E(\lambda)_c$  is not strongly dependent on the actual shape of  $E(\lambda)_c$ , this form applies equally well to cases like HD 63922 which exhibit clear deviations from the  $R(V) = 3.1$  mean extinction law [Fig. 1(a)].

#### 4. SAMPLE EXTINCTION DERIVATION AND ASSOCIATED ERRORS

The most direct way to determine suitability of giants and supergiants for extinction studies is to understand the nature of the combined extinction errors. We group errors into two classes. “Nonselective” errors are those that do not depend upon the spectral type/luminosity class of the program star, while “selective” errors do. Photometric errors and, for the most part, comparison star dereddening errors are nonselective because their magnitude does not depend directly on the nature of the spectra being used. On the other hand, spectral type/luminosity class mismatch errors are selective because their impact on the extinction curve depends upon the intrinsic characteristics of the stars being used. In addition to the general wavelength dependent effects of temperature and luminosity mismatch, the heavy UV line blanketing seen in giant and supergiant spectra can also produce significant localized mismatch errors as seen in the spurious rise in the region of  $\lambda^{-1} \approx 6.3 \mu\text{m}^{-1}$  in the Savage & Mathis (1979) reddening law.

The general sources of uncertainty associated with the pair method can be defined as a combination of nonselective photometric errors (including uncertainties in the observed comparison and program star  $V$ ,  $B - V$ , and zero-point uncertainties in the UV flux distributions), comparison star dereddening errors, and selective temperature and luminosity mismatch errors. The general application of these errors to the derivation of extinction with early-type main-sequence stars has been discussed by MSF and MF. In the discussion below, we follow along some of the general lines of MSF and MF.

The general contribution of the individual uncertainties

can be expressed through a straightforward propagation of errors of  $E(\lambda)$  [ $\equiv E(\lambda - V)/E(B - V)$ ] in the form

$$\sigma[E(\lambda)] = (\sigma[E(\lambda - V)]^2 + \sigma[E(B - V)]^2 E(\lambda)^2)^{1/2} / E(B - V) \quad (1a)$$

with

$$\sigma[E(\lambda - V)] = (\sigma[m(\lambda - V)_p]^2 + \sigma[m_0(\lambda - V)_c]^2)^{1/2}, \quad (1b)$$

where  $m(\lambda - V)_p$  is the observed program star color,  $m_0(\lambda - V)_c [= m(\lambda - V)_c - E(\lambda)_c E(B - V)_c]$  is the *dereddened* comparison star color, and

$$\sigma[m_0(\lambda - V)_c]^2 = \sigma[m(\lambda - V)_c]^2 + \sigma[E(\lambda)_c]^2 E(B - V)_c^2 + \sigma[E(B - V)_c]^2 E(\lambda)_c^2. \quad (1c)$$

It can be shown that these individual error components are generally independent so  $\sigma[E(\lambda)] \approx (\sigma[E(\lambda)_{\text{photometric}}]^2 + \sigma[E(\lambda)_{\text{dereddening}}]^2 + \sigma[E(\lambda)_{\text{mismatch}}]^2)^{1/2}$ . We discuss the photometric, dereddening, and mismatch errors in turn.

#### 4.1 Errors Associated with Photometric Uncertainties

In this section, we consider only the photometric error components in Eqs. (1). The principal photometric measurement error components are  $\sigma[V]$ ,  $\sigma[m(\lambda)]$ , and  $\sigma[B - V]$ . These components are the standard deviations in  $V$ ,  $m(\lambda)$  (the zero-point uncertainty in the *IUE* flux level), and  $B - V$ , respectively. The individual components of the photometric errors are independent, so

$$\sigma[E(\lambda)_{\text{photometric}}] = (\sigma[E(\lambda)_{\text{zero-point}}]^2 + \sigma[E(\lambda)_{\text{color}}]^2)^{1/2}. \quad (2a)$$

By noting that  $\sigma[E(B - V)_c] \approx \sigma[E(B - V)]$ , we have

$$\sigma[E(\lambda)_{\text{zero-point}}] = (\sigma[m(\lambda - V)_p]^2 + \sigma[m(\lambda - V)_c]^2)^{1/2} / E(B - V), \quad (2b)$$

$$\sigma[E(\lambda)_{\text{color}}] = \sigma[E(B - V)] (E(\lambda)_c^2 + E(\lambda)^2)^{1/2} / E(B - V). \quad (2c)$$

Since the comparison and program stars contribute roughly equally to these measurement errors, we have  $\sigma[m(\lambda - V)_p]^2 + \sigma[m(\lambda - V)_c]^2 \approx 2\sigma[V]^2 + 2\sigma[m(\lambda)]^2$  and  $\sigma[E(B - V)] \approx (\sigma(B - V)^2 + \sigma[(B - V)_0]^2)^{1/2}$ . From Bohlin *et al.* (1980) we adopt  $\sigma[m(\lambda)] \approx 0.03$  and from MSF we adopt  $\sigma[V] \approx 0.015$  and  $\sigma(B - V) \approx 0.010$ . For luminosity classes II-Ia, there is some disagreement in  $(B - V)_0$  for a given spectral type (see Fitzpatrick 1988) and so we adopt  $\sigma[(B - V)_0] \approx 0.02$ . We then have

$$\sigma[E(\lambda)_{\text{photometric}}] \approx (0.00225 + 0.0005[E(\lambda)_c^2 + E(\lambda)^2])^{1/2} / E(B - V) \quad (3a)$$

$$\sigma[E(\lambda)_{\text{zero-point}}] \approx 0.047 / E(B - V) \quad (3b)$$

$$\sigma[E(\lambda)_{\text{color}}] \approx 0.022[E(\lambda)_c^2 + E(\lambda)^2]^{1/2} / E(B - V). \quad (3c)$$

TABLE 4. Estimated extinction errors associated with total photometric uncertainties.<sup>a</sup>

$\lambda$ (Å)	$x$ ( $\mu\text{m}^{-1}$ )	$E(\lambda)_{\text{CCM}}^c$	Error Estimates in $\Delta[E(\lambda-V)/E(B-V)]^b$			$\sigma_0^c$
			$E(B-V)^d=0.2$	$E(B-V)^d=0.3$	$E(B-V)^d=0.4$	
3100	3.23	2.4	0.45	0.30	0.22	0.089
2200	4.55	6.6	1.07	0.71	0.54	0.214
1600	6.25	4.7	0.78	0.52	0.39	0.156
1200	8.33	7.9	1.27	0.85	0.64	0.254

Notes to TABLE 4

<sup>a</sup>These “error” estimates include uncertainties in the comparison and program star  $V$ ,  $B-V$ , zero-point  $IUE$  flux, and the adopted  $(B-V)_0$ . The wavelength dependence of the errors is determined and dominated by the color uncertainty through the extinction curve normalization [see Eqs. (3)].

<sup>b</sup>Examples of the relative errors in the derived extinction for three values of program star color excess. These error estimates are coupled in wavelength space through  $E(\lambda)_{\text{CCM}}$  and must be applied with the same relative sign for a given value of  $E(B-V)$ .

<sup>c</sup> $E(\lambda)_{\text{CCM}} = E(\lambda - V)/E(B - V) = R(V)[a(x) - 1] + b(x)$ , the  $R(V)$ -dependent extinction law of Cardelli *et al.* (1989) evaluated for  $R(V) = 3.1$ . These values are representative of extinction observed in diffuse cloud and low density gas (see text). The application of  $E(\lambda)_{\text{CCM}}$  derives from Eq. (3a) assuming  $[E(\lambda)_c^2 + E(\lambda)^2]^{1/2} \approx 2^{1/2}E(\lambda) \approx 2^{1/2}E(\lambda)_{\text{CCM}}$ .

<sup>d</sup>Color excess,  $E(B - V)$ , derived from the comparison between the program and standard star colors.

<sup>e</sup>Photometric error estimates for an arbitrary value of  $E(B - V)$  can be found from  $\sigma_{\text{photometric}} = \sigma_0/E(B - V)$ .

We show general examples of these errors in Table 4 for three different values of  $E(B - V)$ . [We note that the wavelength dependence of these error estimates are coupled and they must be applied with the same relative sign. This wavelength dependence is dominated by the color error as can be seen by evaluating Eqs. (3b) and (3c).] Since  $\sigma[E(\lambda)_{\text{color}}]$  scales like the quadratic sum of the adopted comparison star and derived program star extinction curves, total photometric error values derived from Eq. (3a) or (3c) depend upon the specific program and comparison star extinction. We represent  $E(\lambda)$  by the CCM  $R(V) = 3.1$  extinction curve, which is essentially the same as that of Savage & Mathis (1979) and Seaton (1979), the “mean” curve associated with diffuse interstellar extinction. As will be seen in Sec. 4.3, this curve is also a fair representation of the extinction examples presented here. In addition, it can be shown that for the comparison star dereddening data in Table 2, the adopted  $E(\lambda)_c$  on average are also fairly similar to the CCM  $R(V) = 3.1$  curve. Therefore, we approximate the term  $[E(\lambda)_c^2 + E(\lambda)^2]$  in Eqs. (3a) and (3c) with  $2E(\lambda)_{\text{CCM}}^2$ . The total photometric error estimates in Table 4 are generally applicable to the results discussed below.

#### 4.2 Errors Associated with Comparison Star Dereddening

In Sec. 3.3 we discussed the form of the uncertainty in our adopted comparison star dereddening. The standard deviation arising from dereddening takes the form  $\sigma[E(\lambda)_{\text{dereddening}}] \approx \sigma[E(\lambda)_c]E(B - V)_c/E(B - V) = \sigma[E(\lambda)_c]E_c$ , where  $E_c = E(B - V)_c/E(B - V) \equiv$  the ratio of the comparison star reddening to the total program star

TABLE 5. Estimated extinction errors associated with comparison (standard) star dereddening.

$\lambda$ (Å)	$x$ ( $\mu\text{m}^{-1}$ )	$a(x)$	$\Delta E(\lambda)_c^b$	Error Estimates in $\Delta[E(\lambda-V)/E(B-V)]^a$			$\sigma_0^d$
				$E_c^c = 0.10$	$E_c^c = 0.30$	$E_c^c = 0.50$	
3100	3.23	0.691	0.093	0.01	0.03	0.05	0.093
2200	4.55	0.026	0.292	0.03	0.09	0.15	0.292
1600	6.25	-0.264	0.379	0.04	0.11	0.19	0.379
1200	8.33	-1.292	0.688	0.07	0.21	0.34	0.688

Notes to TABLE 5

<sup>a</sup>Examples of the relative error in the derived program star extinction as a function of the ratio of the comparison star to program star color excess. These error estimates are coupled in wavelength space through  $\Delta E(\lambda)_c$  and must be applied with the same relative sign for a given value of  $E_c$ . <sup>b</sup> $\Delta E(\lambda)_c = \Delta[E(\lambda - V)/E(B - V)]_c = 0.3[a(x) - 1] \equiv$  adopted difference between the “true” and the adopted comparison star reddening curve (see Sec. 3.3).

<sup>c</sup>Ratio of the comparison star to program star color excess,  $E(B - V)_c/E(B - V)$ .

<sup>d</sup>Dereddening error estimates for an arbitrary value of  $E_c$  can be found from  $\sigma_{\text{dereddening}} = \sigma_0 x E_c$ .

reddening. Adopting  $\sigma[E(\lambda)_c] \approx \Delta E(\lambda)_c = \Delta R(V)[a(x) - 1]$  and  $\Delta R(V) \approx 0.3$  (see Sec. 3.3), we find

$$\sigma[E(\lambda)_{\text{dereddening}}] \approx 0.3[a(x) - 1]E_c, \quad (4)$$

where again,  $a(x)$  is taken from CCM. Representative examples of how the adopted comparison star dereddening uncertainties influence the derived extinction,  $E(\lambda)$ , are given in Table 5 at four UV wavelengths for three different values of  $E_c$ . The last column in Table 5 gives general results from Eq. (4) as a function of  $E_c$ . These error estimates are coupled through the wavelength dependence of  $a(x)$  and must be applied with the same relative sign.

#### 4.3 Errors Associated with Luminosity Mismatch

Unlike photometric and dereddening errors, mismatch errors,  $\sigma[E(\lambda)_{\text{mismatch}}]$ , are not as easily evaluated by means of expressions like those in Eqs. (3) and (4), since they depend upon which spectral/luminosity pair of comparison stars are used to assess the mismatch (MF). Properties of mismatch errors of class III-I stars are not as well established as those for class V stars. They are best explored through deliberate and controlled mismatch (i.e., bracketing the “best match” extinction in both luminosity and temperature), similar to the approach employed in Sec. 3.1 to arrive at an estimate of the comparison star reddening. *This is also a practical approach since the sample of comparison stars is limited and temperature and luminosity are not quantized parameters.*

We derive extinction properties for a sample of four giant/supergiant stars which are part of a larger sample of stars being analyzed to determine the nature of extinction in low density disk and halo gas (Cardelli & Sembach 1992; Cardelli *et al.* 1992). The stars discussed here have low to moderately reddening [ $0.2 < E(B - V) < 0.4$ ] and were chosen solely because they cover the range of spectral/luminosity classes considered here. There was no other criterion for their selection. The spectra for each of the four stars are plotted in Fig. 7 along with a comparison

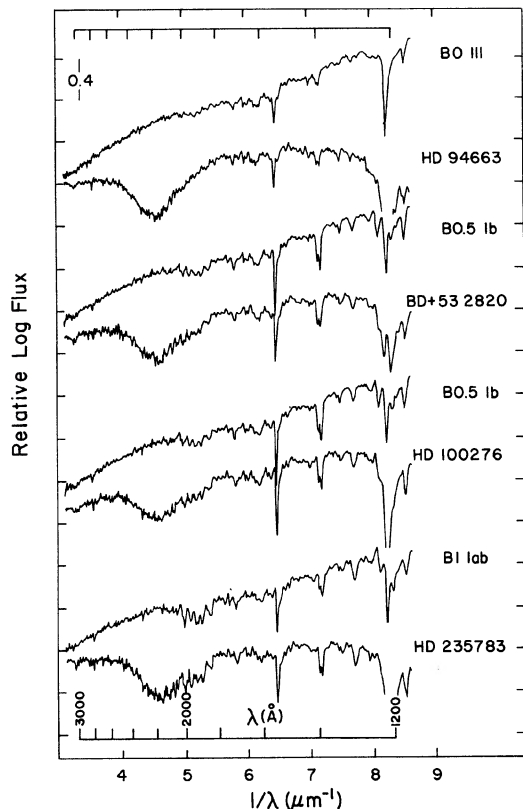


FIG. 7. The logarithm of the relative flux for four program stars taken from Cardelli & Sembach (1992) compared with the “best match” comparison star data (corrected for reddening using the adopted extinction data in Table 2) plotted against  $1/\lambda$  ( $\mu\text{m}^{-1}$ ).

star spectrum that is the *closest match* to the absorption spectrum. For three of the four program stars in Fig. 7, the quoted spectral/luminosity classes derived from optical data are generally the same as the UV classification of our best-match comparison star. However, for BD+53 2820, the quoted optical classification, B0 IV, is inconsistent with the classification B0.5 Ib we infer from the UV data.

The raw (i.e., unbinned/unsmoothed) extinction curves for the four stars, derived from the pairing shown in Fig. 7, are shown in Fig. 8 along with the corresponding values of  $E(B-V)$  and  $E_c$ . The gap in the data at  $x \approx 8.2 \mu\text{m}^{-1}$  occurs at the location of  $L\alpha$  which has been omitted. With the exception of the region around C IV and to a lesser degree Si IV, there is no significant small scale structure, indicating no significant mismatch of the spectral features. The C IV profile is sensitive to differences in the stellar winds that do not necessarily distort the shape of the flux distribution. Such mismatch is not necessarily an indication of uncertainties in the general shape of the curve and mismatch in C IV and to a lesser degree Si IV is generally quite common in early type spectra (FM). However, the C IV lines are also strong and narrow, so the incomplete cancellation is probably also contributed by slight relative

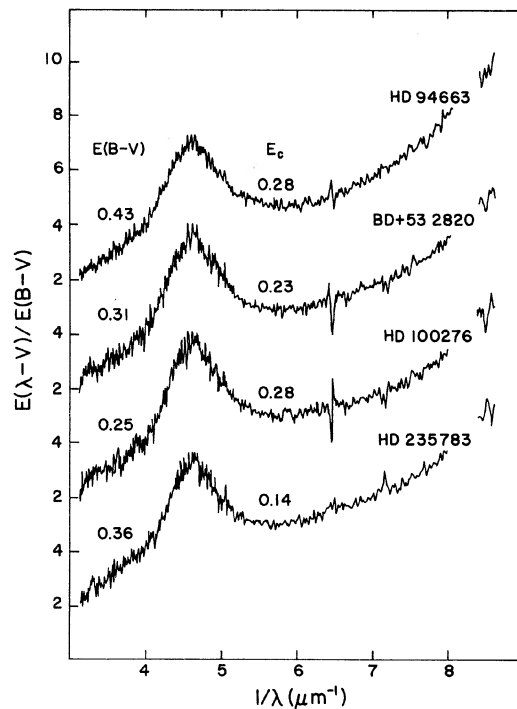


FIG. 8. The raw (unbinned/unsmoothed) extinction curves derived from the program/comparison star pairs shown in Fig. 7, plotted against  $1/\lambda$  ( $\mu\text{m}^{-1}$ ) along with the values of  $E(B-V)$  and  $E_c$ , the ratio of comparison/program star reddening. The gap in the data at  $x \equiv \lambda^{-1} \approx 8.2 \mu\text{m}^{-1}$  occurs at the location of  $L\alpha$  which has been omitted. With the exception of C IV and to a lesser degree Si IV, the other spectral features have completely canceled indicating that the pairs represent good quality matches. For the strong, narrow C IV lines, some of the residual structure is due to slight relative shifts in the central wavelength of the feature between program and comparison star resulting in incomplete cancellation.

shifts in the central wavelength of the feature between program and comparison star.

The lack of obvious spectral mismatch in Fig. 8 does not exclude the possibility of continuum mismatch errors, the effects of other sources of uncertainty like those discussed above, or even errors resulting from differences in the intrinsic characteristics of these stars (such as composition, rotation, etc.). However, the fact that these four curves are very similar suggests that such uncertainties are not large. Since the curves in Fig. 8 depend upon (a) different spectral/luminosity classes, (b) different values of  $E(B-V)$  and  $E_c$ , and (c) different adopted comparison star dereddening, any significant errors or deviations would likely appear in at least one case. The overall similarity of the curves presumably arises because all four sight lines sample dust with similar characteristics.

We are confident that the curves in Fig. 8 are fairly accurate, and they can therefore serve as a basis for exploring the impact of temperature and/or luminosity mismatch. The effects of luminosity mismatch are shown in Fig. 9 for HD 235783. The bottom two plots show the same curve as in Fig. 8 along with the “B1 Iab” compar-

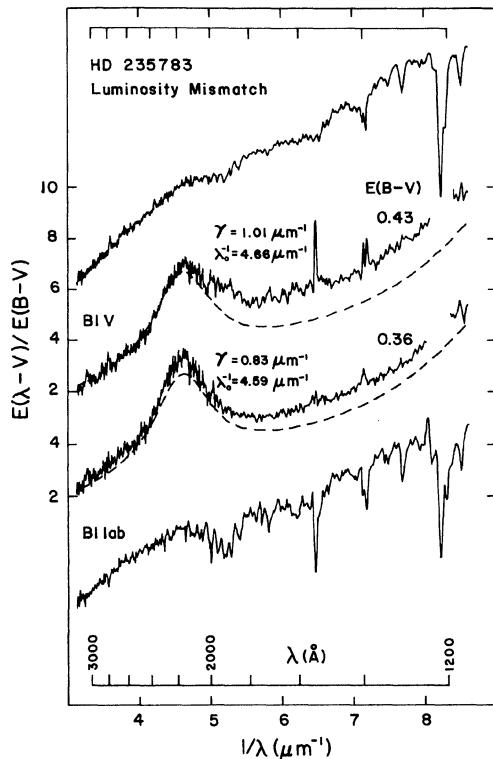


FIG. 9. The middle two plots correspond to the raw (unbinned/unsmoothed) extinction curve for the program star HD 235783 derived from a comparison to the B1 Iab, the “best match” standard star (bottom middle), and to the B1 V (top middle), plotted against  $1/\lambda$  ( $\mu\text{m}^{-1}$ ). The parametrized bump width and central position for these two curves are also shown. For comparison we also display the logarithm of the reddening corrected flux distribution of the B1 Iab (bottom plot) and the B1 V (top plot). Significant structure associated with the mismatch of the absorption spectra can be seen in the curve derived from the B1 V comparison as well as the impact this mismatch has on the fitted  $\gamma$  and  $\lambda_0^{-1}$ .

ison star (HD 91316) from which it was derived. The top two plots show the “B1 V” comparison star (HD 31726) and the corresponding extinction curve. Both the B1 V and B1 Iab spectra are fairly lightly reddened in comparison to HD 235783, and we believe the extinction curve derived from the B1 Iab match to be fairly accurate, so the differences between the two extinction curves should be nearly totally due to luminosity mismatch. (The same argument can be made even if we use the “alternate” classifications as given in Table 3.) Through the peak of the bump, the shapes of the two curves are very similar. However, for  $x > 4.6 \mu\text{m}^{-1}$ , the curve derived from the B1 V comparison is somewhat higher and also contains significant structure. Comparison to the B1 Iab spectra shows this structure to be entirely the result of mismatch of the absorption features. The general elevation of the curve in this region is the result of the B1 V having weaker absorption lines as well as a somewhat steeper continuum than the B1 Iab. The extreme mismatch represented here is easy to identify, especially at the resolution of the *IUE* data, and can there-

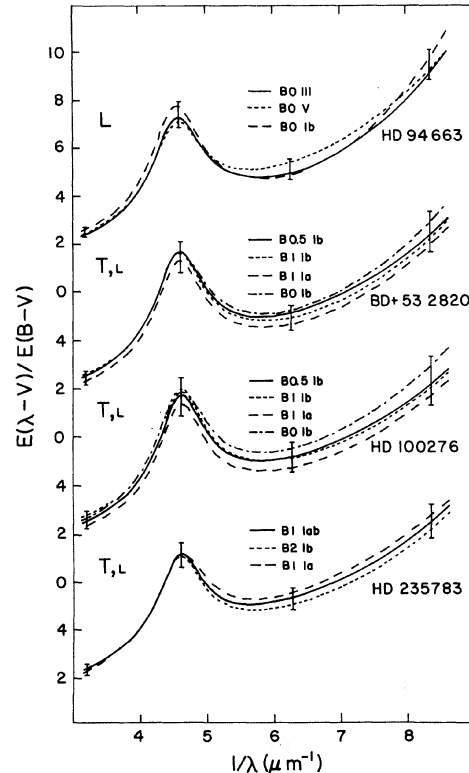


FIG. 10. Fitted extinction curves for the four program stars derived from a comparison to several standards from our sample, plotted against  $1/\lambda$  ( $\mu\text{m}^{-1}$ ), for the purpose of exploring the effects of mismatch. The labels *L* and *T* correspond to the type of mismatch, luminosity or temperature, with the size of the label indicating the more dominant of the two. In each case, the solid line corresponds to the curve derived from the “best match” comparison star (i.e., Fig. 8). The “error bars” correspond to the standard deviations computed from a combination of the photometric and comparison star dereddening error relationships in Eqs. (3a) and (4).

fore be avoided. However, at lower resolution such mismatch could be missed, leading to an incorrect assessment of the extinction curve shape (as was the case for the extinction curve of Savage & Mathis 1979). Such parameters as the bump position and width are also affected by mismatch, as indicated in Fig. 9.

#### 4.4 General Mismatch and Combined Error Assessment

The contribution of the other sources of errors such as those discussed in Secs. 4.1 and 4.2 complicates generalized examples of the spectral/luminosity class mismatch errors discussed in Sec. 4.3. Consequently, we have chosen to examine all sources of error, including general mismatch, for the four curves shown in Fig. 8 and compare these to the estimated errors without mismatch.

The extinction curves for various mismatch cases for the four stars are shown in Fig. 10. The plotted data were derived from fitting the individual computed extinction curves with the parametrization of FM. The corresponding

TABLE 6. Extinction curve fit parameters vs mismatch.

Object	Type <sup>a</sup>	E(B-V) <sub>c</sub> <sup>b</sup>	E(B-V)	E <sub>c</sub> <sup>c</sup>	1/λ <sub>0</sub> <sup>d</sup>	γ <sup>d</sup>	c <sub>1</sub>	c <sub>2</sub>	c <sub>3</sub>	c <sub>4</sub>
HD 94663	B0 III	0.12	0.43	0.28	4.593	0.921	-0.382	0.780	3.447	0.709
	B0 V	0.04	0.43	0.09	4.595	0.910	-0.802	0.931	2.978	0.537
	B0 Ib	0.15	0.36	0.42	4.578	0.910	0.081	0.689	3.731	0.931
σ <sup>e</sup>				<i>0.01</i>	<i>0.01</i>	<i>0.44</i>	<i>0.12</i>	<i>0.38</i>	<i>0.20</i>	
BD+53 2820	B0.5 Ib	0.07	0.31	0.23	4.604	0.893	-0.340	0.804	3.444	0.471
	B1 Ib	0.13	0.29	0.45	4.598	0.899	0.023	0.719	3.447	0.515
	B1 Ia	0.16	0.29	0.55	4.604	0.868	-0.235	0.720	3.169	0.514
	B0 Ib	0.15	0.33	0.45	4.613	0.971	-0.484	0.840	3.942	0.558
	σ <sup>e</sup>				<i>0.01</i>	<i>0.05</i>	<i>0.28</i>	<i>0.06</i>	<i>0.39</i>	<i>0.04</i>
HD 100276	B0.5 Ib	0.07	0.25	0.28	4.607	0.870	-0.318	0.817	3.239	0.397
	B1 Ib	0.13	0.23	0.56	4.606	0.876	0.206	0.725	3.395	0.416
	B1 Ia	0.16	0.23	0.70	4.608	0.845	-0.182	0.731	2.953	0.417
	B0 Ib	0.15	0.27	0.56	4.610	0.952	-0.475	0.891	3.820	0.464
	σ <sup>e</sup>				<i>0.00</i>	<i>0.05</i>	<i>0.34</i>	<i>0.08</i>	<i>0.43</i>	<i>0.03</i>
HD 235783	B1I ab	0.05	0.36	0.14	4.591	0.834	-0.762	0.928	2.586	0.366
	B2 Ib	0.09	0.34	0.26	4.590	0.857	-0.486	0.838	2.726	0.410
	B1 Ia	0.16	0.36	0.44	4.620	0.963	-1.275	1.036	3.370	0.327
σ <sup>e</sup>				<i>0.02</i>	<i>0.06</i>	<i>0.40</i>	<i>0.10</i>	<i>0.39</i>	<i>0.06</i>	
FM standard deviations <sup>f</sup>			0.20	0.03	0.10	0.80	0.19	0.65	0.19	
			0.30	0.02	0.07	0.53	0.11	0.43	0.11	
			0.40	0.01	0.05	0.40	0.09	0.33	0.09	

## Notes to TABLE 6

<sup>a</sup>Quoted optical spectral type of comparison (standard) star used to derive the extinction curve (see Table 1).

<sup>b</sup>Color excess of comparison star. All comparison stars were dereddened using the reddening curve estimates given in Table 2.

<sup>c</sup>Fractional contribution of the comparison star reddening,  $E(B-V)_c$  to the total reddening,  $E(B-V)$ .

<sup>d</sup>Inverse of the fitted bump central wavelength,  $1/\lambda_0$ , and bump width,  $\gamma$ , in  $\mu\text{m}^{-1}$ .

<sup>e</sup>Pseudo-standard deviation defined as the deviation around the mean parameter value.

<sup>f</sup>Empirically derived standard deviations for the various fit parameters for three values of  $E(B-V)$  from the extinction analysis of Fitzpatrick & Massa (1990).

fit parameters are given in Table 6 and discussed below. The solid curves correspond to the fitted results for the best comparison star match (i.e., Fig. 8). The labels “L” and “T” refer to the form of the mismatch (luminosity and/or temperature) with the relative size of the label indicating the relative importance of the two possible effects. The error bars plotted in Fig. 10 correspond to the quadratic addition of photometric and comparison star dereddening uncertainties (see Secs. 4.1 and 4.2). For each case, the errors were estimated for the mean values of  $E(B-V)$  and  $E_c$ .

With the exception of the HD 94663–B0 V comparison, which is an example of fairly excessive mismatch, we employed relatively narrow temperature and/or luminosity mismatch. In this way, we hoped to simulate the type of uncertainties that might actually be incurred in practice if, for example, the quality of the program star data is insufficient to allow an accurate match, and/or the program star data physically represent an intermediate case. The specifics of each case are summarized below.

**HD 94663:** The dominant mismatch for this case corresponds to luminosity class. The major differences between the curves occurs in the region  $5 \mu\text{m}^{-1} < x < 8 \mu\text{m}^{-1}$ . The differences mimic the mismatch effects shown in Fig. 9 and arise from mismatch of the luminosity sensitive absorption features in this region (see Fig. 6).

**BD+53 2820 and HD 100276:** The dominant source of mismatch for these two cases corresponds to temperature

with secondary contributions from luminosity. In both cases, the major deviations occur for  $x > 5 \mu\text{m}^{-1}$  and are generally consistent with what is expected from temperature mismatch in that the curve derived from the earliest spectral type exhibits the highest extinction. However, similar effects are expected from both photometric and dereddening uncertainties. The latter is particularly possible since the values of  $E_c$  are relatively large (see Table 6).

**HD 235783:** The alternate classifications in Table 3 indicate that temperature and to a lesser degree luminosity mismatch contribute in this case. The differences are generally similar to those seen for BD+53 2820 and HD 100276. In particular, for the B1 Ia comparison, the broadening in the bump region is due to mismatch in the “Fe III” absorption (see Fig. 9).

The empirically derived range of extinction curve uncertainties for each case are generally within the standard deviations derived from the estimated sources of error, excluding mismatch, at all wavelengths. Since we know that some mismatch errors *must* be present, these results suggest that they are not a major contributor to the total errors. However, because the deviations of the mismatched curves in Fig. 10 from the “best-match” curve are smaller than our computed errors, the computed errors may be overestimated. We argue that this overestimation cannot be too large by noting that even for cases with  $E_c \approx 0.5$ , the estimated errors are dominated by the photometric color uncertainties, and these uncertainties are fairly well established. We therefore believe that our estimated errors represent reasonable, but possibly conservative, extinction curve uncertainties associated with the use of the comparison stars represented in Fig. 10.

## 5. DISCUSSION/SUMMARY

The results presented above suggest that while extinction derived using giants and supergiants requires more care, the results appear to be as reliable as those derived using main-sequence stars. In Table 6 we present the fit results for the mismatch analysis shown in Fig. 10. For each of the four program star cases, we list in italics the range of deviation about the average parameter value. Also shown at the bottom of the table are the FM standard deviations for the fit parameters for three values of  $E(B-V)$  spanning the range of our analysis. With the exception of  $c_1$  through  $c_4$  for HD 94663, the empirical uncertainty ranges are within the FM standard deviations, which correspond to general extinction errors associated with the use of early type class V stars and include all sources of error. However, even the results for HD 94663 agree if we omit the data for the B0 V curve which we already noted as being an excessive mismatch. Since our analysis has centered on plausible but noticeable limits of temperature and luminosity mismatch, we conclude that the derived extinction data for these four stars are as reliable as any derived from *IUE* data.

The results of the analysis presented in Fig. 10 and Table 6 utilized 7 of our 13 giant and supergiant comparison stars. The consistency of these results within the limits of

both our computed uncertainties and the well-derived FM standard deviations suggests that these comparison stars represent a well-defined, although not necessarily uniform, sequence *and* that our adopted reddening corrections must be reasonable. We argue that the latter must be particularly true since these seven standards comprise a wide range of intrinsic reddening and subsequent large range of  $E_c$  values for the four program stars discussed here. From an analysis similar to that shown in Table 6 and Fig. 10 for other program stars from the sample of Cardelli & Sembach (1992), similar statements can be made about the remaining six giant and supergiant comparison stars.

We conclude that, in conjunction with the adopted dereddening data in Table 2, the set of luminous comparison stars presented here can be used to produce reliable

extinction results provided that care is taken in the matching of spectral features, especially the luminosity-sensitive "Fe III," N IV/C II/Al II, and Fe III/Al III features.

We would like to acknowledge many useful scientific discussions with E. Fitzpatrick and D. Massa and *IUE* data processing issues with J. Nichols-Bohlin. We would also like to thank the *IUE* observatory staff for their help in acquiring and processing the satellite data and an anonymous referee for useful comments and helping us avoid possible misconceptions. J.A.C. and K.R.S. acknowledge support from NASA/*IUE* Grant No. NAG5-832. J.A.C. also acknowledges support from NASA-LTSARP Grant No. NAGW-2520.

#### REFERENCES

- Boggess, A., *et al.* 1978a, *Nature*, 275, 372  
 Boggess, A., *et al.* 1978b, *Nature*, 275, 377  
 Bohlin, R. C., & Holm, A. V. 1980, *IUE/NASA Newsletter*, 10, 37  
 Bohlin, R. C., Holm, A. V., Savage, B. D., Snijders, M. A. J., & Sparks, W. M. 1980, *A&A*, 85, 1  
 Bohlin, R. C., & Grillmair, C. J. 1988a, *ApJS*, 66, 209  
 Bohlin, R. C., & Grillmair, C. J. 1988b, *ApJS*, 68, 487  
 Bohlin, R. C., Harris, A. W., Holm, A. V., & Gry, C. 1990, *ApJS*, 73, 413  
 Cardelli, J. A., & Clayton, G. C. 1991, *AJ*, 101, 1021  
 Cardelli, J. A., Clayton, G. C., & Mathis, J. S. 1989, *ApJ*, 345, 245 (CCM)  
 Cardelli, J. A., & Savage, B. D. 1988, *ApJ*, 325, 864  
 Cardelli, J. A., & Sembach, K. R. 1992, in preparation  
 Cardelli, J. A., Sembach, K. R., & Mathis, J. S. 1992, in preparation  
 Clavel, J., Gilmozzi, R., & Prieto, A. 1988, *A&A*, 191, 392  
 Cousins, A. W. J., & Stoy, R. H. 1962, *Roy. Obs. Bull.*, No. 64  
 FitzGerald, M. P. 1970, *A&A*, 4, 234  
 Fitzpatrick, E. L. 1985, *ApJ*, 299, 219  
 Fitzpatrick, E. L. 1986, *AJ*, 92, 1068  
 Fitzpatrick, E. L. 1988, *ApJ*, 335, 703  
 Fitzpatrick, E. L., & Massa, D. 1986, *ApJ*, 307, 286  
 Fitzpatrick, E. L., & Massa, D. 1988, *ApJ*, 328, 734  
 Fitzpatrick, E. L., & Massa, D. 1990, *ApJS*, 72, 163 (FM)  
 Heck, A. 1987, in *Exploring the Universe with the IUE Satellite*, edited by Y. Kondo (Reidel, Dordrecht), p. 121  
 Hitner, W. A., Garrison, R. F., & Schild, R. E. 1969, *ApJ*, 157, 313  
 Holm, A. V. 1985, *IUE NASA Newsletter*, 26, 11  
 Johnson, H. L. 1955, *Annals d'Ap*, 18, 292  
 Johnson, H. L. 1958, *Lowell Obs. Bull.*, 4, 37  
 Johnson, H. L. 1966, *Comm. Lun. Pl. Obs.*, 4, 99  
 Kester, D. 1981, *A&A*, 99, 375  
 Koornneef, J., & Code, A. D. 1981, *ApJ*, 247, 860  
 Lesh, J. R. 1968, *ApJS*, 17, 371  
 Lindemann, E. & Hauck, B. 1973, *A&AS*, 11, 119  
 Massa, D. 1989, *AA*, 224, 131  
 Massa, D., & Fitzpatrick, E. L. 1986, *ApJS*, 60, 305 (MF)  
 Massa, D., Savage, B. D., & Fitzpatrick, E. L. 1983, *ApJ*, 266, 662 (MSF)  
 Mathis, J. S., & Cardelli, J. A. 1992, *ApJ* (in press)  
 Nandy, K., Thompson, G. I., Jamar, C., Monfils, A., & Wilson, R. 1976, *A&A*, 52, 63  
 Nandy, K., Morgan, D. H., Willis, A. J., Wilson, R., & Gondhalekar, P. M. 1981, *MNRAS*, 196, 955  
 Nicolet, B. 1978, *A&AS*, 34, 1  
 Panek, R. J., & Savage, B. D. 1976, *ApJ*, 206, 167  
 Prinja, R. K. 1990, *MNRAS*, 246, 392  
 Savage, B. D., Massa, D., Meade, M. R., & Wesselius, P. R. 1985, *ApJS*, 59, 397  
 Savage, B. D., & Mathis, J. S. 1979, *ARA&A*, 17, 73  
 Seaton, M. J. 1979, *MNRAS*, 187, 73p  
 Sonneborn, G., & Garhart, M. P. 1987, *NASA/IUE Newsletter*, 33, 78  
 Turnrose, E. B., & Thompson, R. W. 1984, *IUE Image Processing Information Manual Version 2.0* (Computer Sci. Corp: TM-84/6058)  
 Walborn, N. R. 1971, *ApJS*, 23, 257  
 Walborn, N. R. 1972, *AJ*, 77, 312  
 Walborn, N. R. 1973, *AJ*, 78, 1067  
 Wu, C.-C., *et al.* 1983, *IUE Ultraviolet Spectral Atlas*, *IUE/NASA Newsletter* No. 22  
 Wu, C.-C., Faber, S. M., Gallagher, J. S., Peck, M., & Tinsley, B. M. 1980, *ApJ*, 237, 290